applied sciences

MDPI

Article

Texture-Based Analysis of ^{18}F-Labeled Amyloid PET Brain Images

Alexander P. Seiffert [1,*], Adolfo Gómez-Grande [2], Eva Milara [1], Sara Llamas-Velasco [3,4,5], Alberto Villarejo-Galende [3,4,5,6], Enrique J. Gómez [1,7] and Patricia Sánchez-González [1,7,*]

1 Biomedical Engineering and Telemedicine Centre, ETSI Telecomunicación, Center for Biomedical Technology, Universidad Politécnica de Madrid, 28040 Madrid, Spain; eva.milara.hernando@alumnos.upm.es (E.M.); enriquejavier.gomez@upm.es (E.J.G.)
2 Department of Nuclear Medicine, Hospital Universitario 12 de Octubre, 28041 Madrid, Spain; adolfo.gomez@salud.madrid.org
3 Department of Neurology, Hospital Universitario 12 de Octubre, 28041 Madrid, Spain; sara.llamas@salud.madrid.org (S.L.-V.); alberto.villarejo@salud.madrid.org (A.V.-G.)
4 Group of Neurodegenerative Diseases, Hospital 12 de Octubre Research Institute (imas12), 28041 Madrid, Spain
5 Biomedical Research Networking Center in Neurodegenerative Diseases (CIBERNED), 28029 Madrid, Spain
6 Facultad de Medicina, Universidad Complutense de Madrid, 28040 Madrid, Spain
7 Centro de Investigación Biomédica en Red de Bioingeniería, Biomateriales y Nanomedicina (CIBER-BBN), 28029 Madrid, Spain
* Correspondence: ap.seiffert@upm.es (A.P.S.); p.sanchez@upm.es (P.S.-G.)

Abstract: Amyloid positron emission tomography (PET) brain imaging with radiotracers like [^{18}F]florbetapir (FBP) or [^{18}F]flutemetamol (FMM) is frequently used for the diagnosis of Alzheimer's disease. Quantitative analysis is usually performed with standardized uptake value ratios (SUVR), which are calculated by normalizing to a reference region. However, the reference region could present high variability in longitudinal studies. Texture features based on the grey-level co-occurrence matrix, also called Haralick features (HF), are evaluated in this study to discriminate between amyloid-positive and negative cases. A retrospective study cohort of 66 patients with amyloid PET images (30 [^{18}F]FBP and 36 [^{18}F]FMM) was selected and SUVRs and 6 HFs were extracted from 13 cortical volumes of interest. Mann–Whitney U-tests were performed to analyze differences of the features between amyloid positive and negative cases. Receiver operating characteristic (ROC) curves were computed and their area under the curve (AUC) was calculated to study the discriminatory capability of the features. SUVR proved to be the most significant feature among all tests with AUCs between 0.692 and 0.989. All HFs except correlation also showed good performance. AUCs of up to 0.949 were obtained with the HFs. These results suggest the potential use of texture features for the classification of amyloid PET images.

Keywords: Alzheimer's disease; amyloid PET; florbetapir; flutemetamol; Haralick features; grey-level co-occurrence matrix; texture analysis; SUVR

Citation: Seiffert, A.P.; Gómez-Grande, A.; Milara, E.; Llamas-Velasco, S.; Villarejo-Galende, A.; Gómez, E.J.; Sánchez-González, P. Texture-Based Analysis of ^{18}F-Labeled Amyloid PET Brain Images. *Appl. Sci.* **2021**, *11*, 1991. https://doi.org/10.3390/app11051991

Academic Editor: Gloria Bueno

Received: 17 January 2021
Accepted: 20 February 2021
Published: 24 February 2021

1. Introduction

Amyloid-beta (Aβ) plaques are established as one of the two main biomarkers of Alzheimer's disease (AD) [1]. The abnormal extracellular deposition of Aβ results in neuronal dysfunction and could lead to neuronal death [2]. Positron emission tomography (PET) imaging with Aβ-binding tracers, like [^{11}C]Pittsburgh compound-B (PiB) [3], [^{18}F]florbetapir (FBP) [4], [^{18}F]florbetaben (FBB) [5] and [^{18}F]flutemetamol (FMM) [6], allow for the in-vivo evaluation of its deposition in the brain. Generally, ^{18}F-labeled tracers are used more commonly in clinical practice due to their increased half-life compared to ^{11}C-labeled tracers [7].

The interpretation of amyloid PET images is performed visually in clinical practice and is defined in the Society of Nuclear Medicine and Molecular Imaging (SNMMI) procedure

standard/European Association of Nuclear Medicine (EANM) practice guideline [8]. The main feature for the visual classification is the grey-to-white matter contrast in amyloid PET images. Cases of abnormally elevated cortical Aβ deposition are considered amyloid-positive (Aβ+). The difference between both regions is difficult to identify and the image intensities are more homogeneous. Amyloid-negative (Aβ−) cases are characterized by slight white matter uptake without grey matter uptake. White matter can be clearly differentiated and the image intensity distribution between both tissues is heterogeneous.

The visual analysis and classification of amyloid PET images are recommended by the manufacturers and are performed in clinical practice. It must be noted that amyloid PET imaging is currently only considered a diagnostic biomarker and the corresponding radiotracers have been approved for clinical use for visual interpretation and to classify images as Aβ+ or Aβ− [1,9,10]. The sensitivity of the visual analysis of amyloid PET images when differentiating healthy control subjects from those with mild cognitive impairment (MCI) or AD is over 90% [11]. However, borderline cases that are difficult to classify visually could require quantitative analysis. Thresholds for the classification between amyloid-positive and amyloid-negative based on the standardized uptake value (SUV) have been calculated for all Aβ-binding tracer, namely [^{11}C]PiB [12], [^{18}F]FBP [13], [^{18}F]FBB [5] and [^{18}F]FMM [14]. The progression of amyloid deposition as seen in PET images is also studied and its relationship to cognitive functions [15].

Even though the quantitative analysis of Aβ-binding tracer uptake in PET images is focused on the SUV, visual analysis is still the gold standard in clinical settings [8]. Moreover, it presents limitations and other approaches have previously been proposed. These are mainly motivated by finding an alternative to the reference region normalization, which has shown high variability in longitudinal studies [16,17] and its optimization has been studied for different radiotracers [18–20]. Whittington and Gunn [21] presented an imaging biomarker called amyloid load, which quantifies the Aβ burden from 0% to 100%. Another quantification approach evaluated previously is the textural analysis of amyloid PET images. Campbell et al. [22] studied group differences of textural features and SUV ratios (SUVR) of cortical brain regions in patients of different clinical factors. The authors demonstrated statistically significant differences in textural features between the study groups. Ben Bouallègue et al. [23] evaluated the diagnostic and prognostic value of textural and shape features in amyloid PET images. Textural features are shown to be able to be used for the prediction of the conversion from mild cognitive impairment to AD. However, differences between textural features of amyloid-positive and amyloid-negative PET images have not been studied.

The goal of this study is to evaluate the usefulness of textural image features for the classification of positive or negative PET amyloid images, especially compared to the more common SUVR. Textural image analysis is based on the Haralick features (HF) [24], which are obtained from the grey level co-occurrence matrix (GLCM) and quantify the spatial distribution of image intensities. The features are studied whether they can correctly describe the grey-to-white matter contrast and their discriminatory performance is evaluated and compared to the more conventional SUVR.

2. Materials and Methods

2.1. Subjects

The study cohort was retrospectively selected from patients with clinical diagnoses of neurodegenerative disease, and who were transferred to the department of nuclear medicine for PET/CT brain imaging. Patients who had undergone an amyloid PET scan were included. Amyloid PET images were acquired either with [^{18}F]FBP or [^{18}F]FMM. The subjects are divided into two groups according to the employed amyloid tracer. Amyloid positivity or negativity was evaluated visually by specialists in Nuclear Medicine. The demographic characteristics are shown in Table 1.

Table 1. Demographics of the study group.

	N	Age (y ± SD)	Gender (m/f)	Amyloid Positive/Negative
Amyloid imaging with [^{18}F]FBP	30	66.46 ± 8.76	19/11	16/14
Amyloid imaging with [^{18}F]FMM	36	62.72 ± 7.69	15/21	25/11
Total	66	66.11 ± 8.06	21/25	41/25

2.2. Image Acquisition

Amyloid PET images were acquired based on [^{18}F]FBP or [^{18}F]FMM on a Siemens Biograph 6 True Point PET/CT scanner (Siemens Healthineers AG, Erlangen, Germany). For [^{18}F]FBP imaging, a dose of 360 ± 47 MBq was administered intravenously and the images were recorded 44–92 min post-injection. On the other hand, the dose of [^{18}F]FMM was 189 ± 21 MBq and the image acquisition started 80–138 min post-injection. A point spread function (PSF) reconstruction algorithm was used (three iterations, 21 subsets, all-pass filter) and the images were corrected for attenuation with a low-dose CT scan. Scatter and random correction were also performed. The reconstructed images had a matrix size of 168 × 168 × 33 and voxel size of 4.0728 × 4.0728 × 5 mm^3.

2.3. Image Analysis

All images are preprocessed using Statistical Parametric Mapping 12 (SPM12) (Wellcome Centre for Human Neuroimaging, University College London, London, UK) [25]. Preprocessing includes a manual orientation of the PET/CT images, coregistration between PET and CT images, spatial normalization to the Montreal Neurological Institute (MNI) space based on the unified segmentation algorithm of SPM12 using the CT image as an anatomical reference [26], and segmentation of cortical brain regions. Spatially normalized PET images have a matrix size of 91 × 109 × 91 and voxel size of 2 × 2 × 2 mm^3.

The segmentation of cortical brain regions for the textural analysis is based on the Automatic Anatomical Labelling (AAL2) atlas [27,28]. This way, 6 volumes of interest (VOI) are defined for each brain hemisphere due to potential asymmetry of the amyloid burden [29,30], corresponding to the frontal, occipital, parietal and temporal lobes, the combined posterior cingulate/precuneus (PCC) and the anterior cingulate. These 6 VOIs are selected based on the specifications of the visual interpretation [8–10]. Additionally, a global VOI is defined as the sum of the 12 VOIs. Spatially normalized images are segmented by these VOIs as the goal is to study the difference between grey matter and white matter image intensities, except in the case of SUV calculations where a previous grey matter segmentation is performed. The AAL2 segmentation provides regions with higher cortical thickness and is, therefore, best-suited for the proposed analysis. For each region, the 3-dimensional (3D) GLCM is constructed. The process is based on the Radiomics toolbox (https://github.com/mvallieres/radiomics, accessed on 23 February 2021) by M. Vallières for MATLAB (The MathWorks Inc., Natick, MA, USA) [31–33]. Before GLCM computation, image intensities are quantized into 128 bins using equal probability quantization. A total of 6 HFs are calculated, namely energy, contrast, entropy, homogeneity, correlation, and dissimilarity [24,33], which have previously been used while analyzing amyloid PET images and have shown good performance [22,23]. On the other hand, the SUVRs are obtained by normalizing the average SUV of each region to the average SUV of the grey matter part of the cerebellum [8,14,34].

2.4. Statistical Analysis

Quantitative variables are represented as mean ± standard deviation. Statistical testing is performed to evaluate differences between quantitative features of Aβ+ and Aβ− PET images. Differences between groups are evaluated using Mann–Whitney U-

tests. Receiver characteristic curves (ROC) are computed and the area under the curve (AUC) is used to quantify the discriminatory performance of the image feature. AUC values > 0.7 or <0.3 (inverse relationship between feature value and the positive class) are considered to describe acceptable discrimination [35]. A total of 273 statistical tests are performed (3 subgroups, 13 VOIs, 7 image features). For a group of VOIs and image features, False Discovery Rate (FDR) is controlled at level 0.05 based on the Benjamini–Hochberg procedure to adjust for multiple comparisons. All data are statistically analyzed on SPSS software version 19.00 (IBM Corp., Armonk, NY, USA).

3. Results

Results from the Mann–Whitney U-test using global features are shown in Table 2. When comparing image features between Aβ+ and Aβ− patients independently of the used radiotracer and in the [^{18}F]FBP group, all features show statistically significant differences except one. Correlation does not show significant differences between Aβ+ and Aβ− in any of the study groups (p = 0.037, p = 0.022 and p = 0.295, respectively). Additionally, energy and contrast are not significant features when analyzing the images acquired with [^{18}F]FMM (p = 0.057 and p = 0.029, respectively).

Table 2. Differences between global image features of Aβ+ and Aβ− cases evaluated by Mann–Whitney U-tests. Significant False Discovery Rate (FDR)-adjusted p-values are given in bold.

Image Feature	All Patients	[^{18}F]FBP	[^{18}F]FMM
SUVR	**<0.001**	**0.011**	**<0.001**
Energy	**<0.001**	**0.001**	0.057
Contrast	**<0.001**	**0.001**	0.029
Entropy	**<0.001**	**0.001**	**0.019**
Homogeneity	**<0.001**	**0.001**	**0.019**
Correlation	0.037	0.022	0.295
Dissimilarity	**<0.001**	**0.001**	**0.027**

The results for the analyses of the individual VOIs for the three study groups are shown in Tables 3–5, respectively. Across all VOIs, the SUVR shows significant differences between Aβ+ and Aβ− for all three study groups, except in the occipital and left parietal VOIs in [^{18}F]FBP images. Regarding HFs, energy and homogeneity show significant differences in 9 VOIs (all except the parietal and left anterior cingulate VOIs) for all patients, more than any other HF in that study group. In the case of [^{18}F]FBP PET images, homogeneity is significantly different in 7 VOIs (left and right frontal and occipital VOIs, as well as the left PCC and right temporal and anterior cingulate VOIs). When analyzing only [^{18}F]FMM PET images energy also shows significant differences in 7 VOIs (occipital, temporal and PCC, as well as right anterior cingulate VOIs).

Table 3. Differences between volumes of interest (VOI) image features of Aβ+ and Aβ− of all cases evaluated by Mann–Whitney U-tests. Significant p-values after FDR correction are given in bold. (L, left; R, right; PCC, combined posterior cingulate/precuneus).

Image Feature	Frontal		Occipital		Parietal		Temporal		PCC		Anterior Cingulate	
	L	R	L	R	L	R	L	R	L	R	L	R
SUVR	**<0.001**	**<0.001**	**0.005**	**0.007**	**0.003**	**0.001**	**0.001**	**<0.001**	**<0.001**	**<0.001**	**<0.001**	**0.003**
Energy	**0.020**	**0.002**	**<0.001**	**<0.001**	0.253	0.776	**0.003**	**0.001**	**0.032**	**<0.001**	0.574	**<0.001**
Contrast	**0.001**	**<0.001**	**<0.001**	**<0.001**	0.130	0.092	**0.005**	**0.013**	**<0.001**	**<0.001**	0.556	0.890
Entropy	**<0.001**	**<0.001**	**<0.001**	**<0.001**	0.130	0.548	**0.023**	**0.007**	0.117	**<0.001**	0.592	**0.001**
Homogeneity	**0.008**	**<0.001**	**<0.001**	**<0.001**	0.188	0.786	**0.001**	**<0.001**	**<0.001**	**<0.001**	0.054	**<0.001**
Correlation	0.232	**0.012**	0.087	0.416	0.539	0.226	**<0.001**	**0.020**	0.092	0.697	0.488	**0.001**
Dissimilarity	**0.001**	**<0.001**	**<0.001**	**<0.001**	0.130	0.207	**0.002**	**0.005**	**<0.001**	**<0.001**	0.817	0.163

Table 4. Differences between VOI image features of Aβ+ and Aβ− of [^{18}F]FBP cases evaluated by Mann–Whitney U-tests. Significant *p*-values after FDR correction are given in bold. (L, left; R, right; PCC, combined posterior cingulate/precuneus).

Image Feature	Frontal		Occipital		Parietal		Temporal		PCC		Anterior Cingulate	
	L	R	L	R	L	R	L	R	L	R	L	R
SUVR	**0.003**	**0.010**	0.031	0.074	0.074	**0.018**	**0.016**	**0.003**	**0.002**	**0.005**	**0.002**	0.025
Energy	0.067	**0.002**	**0.010**	0.034	0.383	0.280	0.383	0.146	**0.009**	0.034	0.454	**0.009**
Contrast	**0.003**	**0.001**	0.028	0.051	0.088	0.056	0.124	0.406	**0.010**	0.022	0.803	0.618
Entropy	**0.002**	**<0.001**	**0.018**	0.025	0.198	0.170	0.708	0.589	**0.005**	0.025	0.454	**0.006**
Homogeneity	**0.011**	**0.001**	**0.008**	**0.009**	0.280	0.212	0.081	**0.067**	**0.018**	0.046	0.105	**0.001**
Correlation	0.124	0.028	0.406	0.618	0.212	0.198	0.022	0.056	0.170	0.360	0.708	0.212
Dissimilarity	**0.004**	**0.001**	0.025	**0.018**	0.124	0.114	0.124	0.299	**0.016**	0.022	0.967	0.114

Table 5. Differences between VOI image features of Aβ+ and Aβ− of [^{18}F]FMM cases evaluated by Mann–Whitney U-tests. Significant *p*-values after FDR correction are given in bold. (L, left; R, right; PCC, combined posterior cingulate/precuneus).

Image Feature	Frontal		Occipital		Parietal		Temporal		PCC		Anterior Cingulate	
	L	R	L	R	L	R	L	R	L	R	L	R
SUVR	**<0.001**	**<0.001**	**<0.001**	**0.001**	**<0.001**	**<0.001**	**<0.001**	**<0.001**	**<0.001**	**<0.001**	**<0.001**	**<0.001**
Energy	0.175	0.236	**<0.001**	**<0.001**	0.440	0.144	**0.006**	**0.004**	**<0.001**	**<0.001**	0.525	**0.005**
Contrast	0.038	**0.009**	**<0.001**	**0.001**	0.328	0.363	0.035	**0.009**	**0.010**	**<0.001**	0.718	0.986
Entropy	**0.022**	0.052	**<0.001**	**0.001**	0.236	0.718	0.032	**0.003**	**<0.001**	**<0.001**	0.503	0.035
Homogeneity	0.135	0.110	**<0.001**	**<0.001**	0.295	0.481	**0.002**	**0.003**	**0.003**	**<0.001**	0.090	0.035
Correlation	0.904	0.175	0.118	0.400	0.850	0.279	**0.009**	0.061	0.932	0.823	0.250	**0.001**
Dissimilarity	0.035	**0.024**	**<0.001**	**<0.001**	0.295	0.503	**0.012**	**0.006**	**0.006**	**<0.001**	0.932	0.503

On the other hand, all image features are significantly different between Aβ+ and Aβ− in the right frontal and temporal VOIs when grouping all patients. In [^{18}F]FBP, the regions with the most significant features are the right frontal lobe (all except correlation, $p = 0.028$) and left PCC (all except correlation, $p = 0.170$. In the [^{18}F]FMM study group, 5 VOIs show significant differences between Aβ+ and Aβ− for all features except correlation (occipital and PCC VOIs, as well as the right temporal VOI).

ROC curves of the image features using the global VOI for each study group are shown in Figure 1 and their corresponding AUC values in Table 6. The SUVR shows the best discriminatory capabilities with the highest AUC in the [^{18}F]FMM study groups (0.96) while homogeneity performs better in the other two groups (0.813 and 0.862, respectively). Except in the case of SUVR, AUC values are higher in the study group of patients whose amyloid PET images were acquired with [^{18}F]FBP. Lastly, only correlation results in an AUC value < 0.7. In the study group of all patients, the AUC is 0.654. When analyzing only the [^{18}F]FMM study group, homogeneity results in an AUC value of 0.611.

Table 6. Area under the curve (AUC) values from ROC analyses for the three study groups. AUCs > 0.7 and <0.3 are given in bold.

Image Feature	All Patients	[^{18}F]FBP	[^{18}F]FMM
SUVR	**0.758**	**0.772**	**0.960**
Energy	**0.785**	**0.844**	**0.702**
Contrast	**0.203**	**0.143**	**0.269**
Entropy	**0.181**	**0.134**	**0.251**
Homogeneity	**0.813**	**0.862**	**0.749**
Correlation	0.654	**0.746**	0.611
Dissimilarity	**0.194**	**0.129**	**0.265**

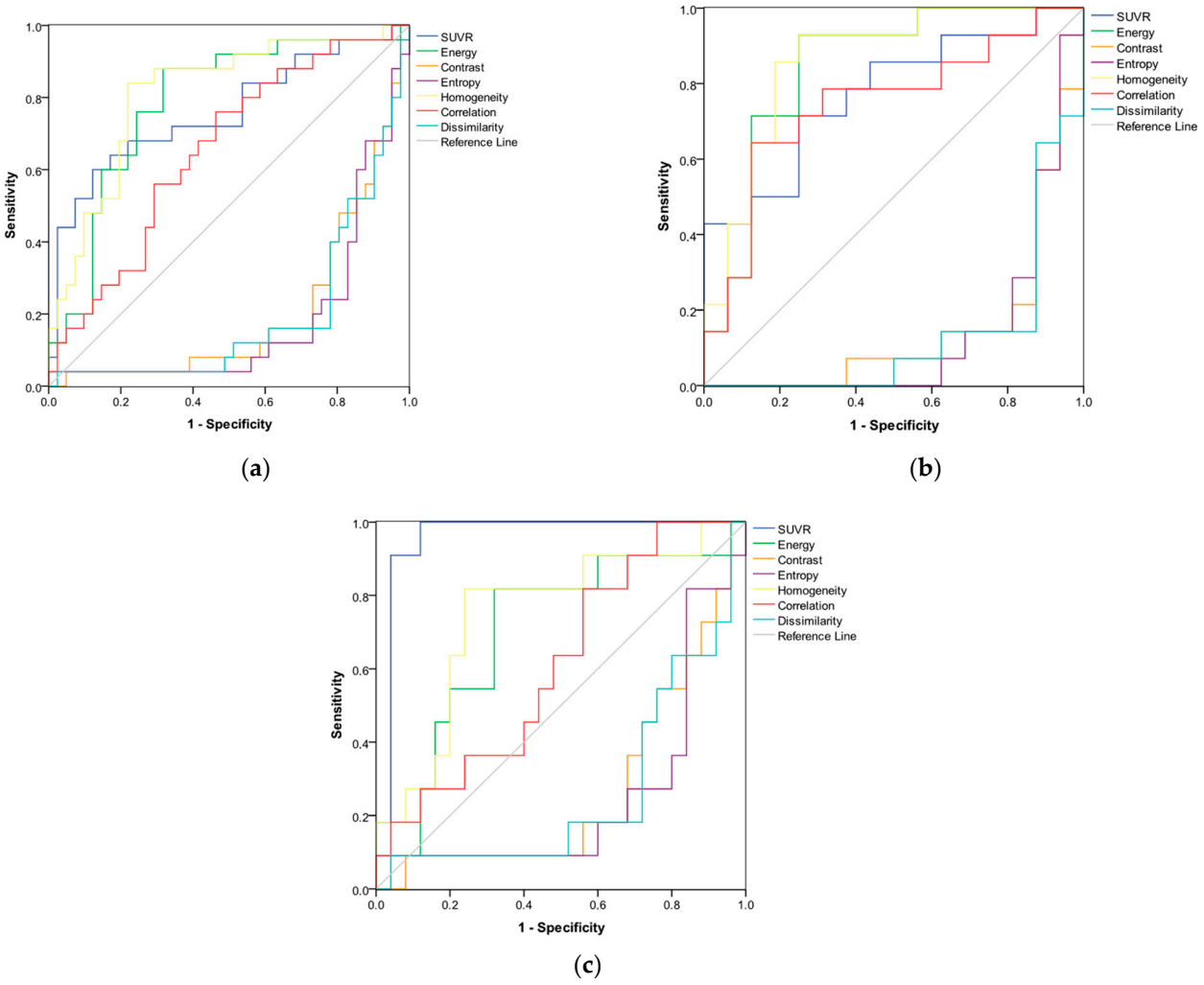

Figure 1. Receiver characteristic curves (ROC) curves representing the discriminatory capacity of the global standardized uptake value ratios (SUVR) and Haralick features (HFs) in separating Aβ+ and Aβ− cases. ROC curves for the three study groups: (**a**) all patients; (**b**) amyloid positron emission tomography (PET) images acquired with [^{18}F]FBP; (**c**) amyloid PET images acquired with [^{18}F]FMM.

AUC values from ROC curves of the individual VOIs for the first study group are shown in Table 7. In the first study group with all cases, the SUVR shows in all VOIs AUCs > 0.7, except the left occipital VOI (0.698). The highest AUC is obtained with energy in the left occipital VOI (0.880). Additionally, dissimilarity shows AUC values > 0.7 or <0.3 in 8 VOIs (all except parietal and anterior cingulate VOIs). On the other hand, 6 of the 7 image features result in high AUC values in the right frontal, left occipital and temporal VOIs, as well as the right PCC, more than any other region.

Tables 8 and 9 show the AUC values of the image features in the study groups after separating into images acquired with [^{18}F]FBP and [^{18}F]FMM. While image features extracted from the global VOI show better discriminatory performance in the [^{18}F]FBP group than [^{18}F]FMM, this trend is generally inversed when computing ROC curves with features from regional VOIs. Grouped by radiotracer, SUVR again results in AUC values > 0.7 in nearly every VOI, indicating that higher SUVRs are related to Aβ+. An exception are the right occipital (as in the previous study group) and left parietal VOIs in the [^{18}F]FBP group. Moreover, the overall highest AUC is obtained with the SUVR in the left temporal VOI of the [^{18}F]FMM group (0.989). Excluding the SUVR, the largest AUC is obtained also in the [^{18}F]FMM group with energy in the right PCC VOI. The HF with the most VOIs (9 out of 12) with AUC values < 0.3 is entropy in the [^{18}F]FMM group. Lastly,

all features in the right frontal VOI of the [^{18}F]FBP images and in the left temporal VOI of the [^{18}F]FMM group present AUC values > 0.7 or <0.3. Moreover, 3 VOIs (left occipital and PCC) in the [^{18}F]FBP group and 5 VOIs (occipital, right temporal and PCC) in the [^{18}F]FMM group result in AUC values > 0.7 or <0.3 with 6 out of 7 image features. In all cases, only correlation shows AUC values < 0.7.

Table 7. AUC values from ROC analyses of VOI image features for all patients. AUCs > 0.7 and <0.3 are given in bold. (L, left; R, right; PCC, combined posterior cingulate/precuneus).

Image Feature	Frontal		Occipital		Parietal		Temporal		PCC		Anterior Cingulate	
	L	R	L	R	L	R	L	R	L	R	L	R
SUVR	**0.772**	**0.768**	**0.705**	0.698	**0.717**	**0.745**	**0.747**	**0.775**	**0.787**	**0.768**	**0.788**	**0.720**
Energy	0.671	**0.730**	**0.880**	**0.837**	0.584	0.479	**0.722**	**0.738**	0.659	**0.811**	0.541	**0.767**
Contrast	**0.249**	**0.183**	**0.187**	**0.178**	0.388	0.376	**0.295**	0.316	**0.212**	**0.223**	0.543	0.490
Entropy	**0.231**	**0.203**	**0.152**	**0.167**	0.388	0.456	0.333	0.301	0.384	**0.172**	0.460	**0.264**
Homogeneity	0.696	**0.768**	**0.864**	**0.858**	0.597	0.520	**0.773**	**0.769**	**0.780**	**0.799**	0.642	**0.777**
Correlation	0.588	0.685	0.626	0.560	0.545	0.589	**0.758**	0.671	0.624	0.529	0.449	**0.260**
Dissimilarity	**0.249**	**0.194**	**0.167**	**0.159**	0.388	0.407	**0.266**	**0.294**	**0.211**	**0.210**	0.517	0.397

Table 8. AUC values from ROC analyses of VOI image features from [^{18}F]FBP PET images. AUCs > 0.7 and <0.3 are given in bold. (L, left; R, right; PCC, combined posterior cingulate/precuneus).

Image Feature	Frontal		Occipital		Parietal		Temporal		PCC		Anterior Cingulate	
	L	R	L	R	L	R	L	R	L	R	L	R
SUVR	**0.768**	**0.777**	**0.732**	0.692	0.692	**0.754**	**0.759**	**0.817**	**0.835**	**0.799**	**0.826**	**0.741**
Energy	0.696	**0.826**	**0.777**	**0.728**	0.594	0.616	0.594	0.656	**0.781**	**0.728**	0.580	**0.781**
Contrast	**0.183**	**0.138**	**0.263**	**0.290**	0.317	**0.295**	0.335	0.411	**0.223**	**0.254**	0.527	0.446
Entropy	**0.161**	**0.125**	**0.246**	**0.259**	0.362	0.353	0.460	0.442	**0.196**	**0.259**	0.420	**0.205**
Homogeneity	**0.732**	**0.848**	**0.786**	**0.781**	0.616	0.634	0.687	0.696	**0.754**	**0.714**	0.674	**0.844**
Correlation	0.665	**0.737**	0.589	0.554	0.634	0.638	**0.746**	**0.705**	0.647	0.598	0.540	0.366
Dissimilarity	**0.192**	**0.134**	**0.259**	**0.246**	0.335	0.330	0.335	0.388	**0.241**	**0.254**	0.496	0.330

Table 9. AUC values from ROC analyses of VOI image features from [^{18}F]FMM PET images. AUCs > 0.7 and <0.3 are given in bold. (L, left; R, right; PCC, combined posterior cingulate/precuneus).

Image Feature	Frontal		Occipital		Parietal		Temporal		PCC		Anterior Cingulate	
	L	R	L	R	L	R	L	R	L	R	L	R
SUVR	**0.971**	**0.935**	**0.880**	**0.851**	**0.920**	**0.924**	**0.989**	**0.978**	**0.964**	**0.945**	**0.964**	**0.956**
Energy	0.644	0.625	**0.942**	**0.873**	0.582	0.345	**0.789**	**0.807**	**0.927**	**0.949**	0.567	**0.796**
Contrast	**0.280**	**0.222**	**0.105**	**0.138**	0.396	0.404	**0.276**	**0.222**	**0.225**	**0.124**	0.538	0.502
Entropy	**0.258**	**0.295**	**0.091**	**0.138**	0.375	0.538	**0.273**	**0.185**	**0.076**	**0.025**	0.429	**0.276**
Homogeneity	0.658	0.669	**0.924**	**0.902**	0.611	0.425	**0.825**	**0.815**	**0.818**	**0.916**	0.680	**0.724**
Correlation	0.513	0.644	0.665	0.589	0.520	0.615	**0.778**	0.698	0.509	0.476	0.378	**0.153**
Dissimilarity	**0.276**	**0.262**	**0.080**	**0.124**	0.389	0.429	**0.233**	**0.211**	**0.207**	**0.109**	0.509	0.429

4. Discussion

In this study, image features from ^{18}F-labeled amyloid PET images are evaluated to differentiate between Aβ+ and Aβ− cases. The SUVR, commonly used in clinical practice, as well as 6 HFs, which do not require a reference region normalization, are extracted. The quantitative features are compared in three study groups. These correspond to all the patients of the retrospective cohort, those whose amyloid PET images were acquired with [^{18}F]FBP, and [^{18}F]FMM PET images. Each HF is evaluated individually whether it can

describe quantitatively the grey-to-white matter contrast present in Aβ− images compared to its decrease in Aβ+ cases.

Statistical testing revealed that the SUVR is still the best feature when discriminating between Aβ+ and Aβ− PET images, showing significant differences in all regions and study groups except in 3 VOIs of the [^{18}F]FBP group. Cut-offs have been previously defined for different amyloid-binding radiotracers [5,12–14] and the SUV is also used in clinical practice for quantifying PET images. However, all HFs showed significant differences in at least 3 VOIs in every study group. An exception is correlation, which is found to not be a useful image feature in our study. Even though grey and white matter present similar voxel intensities in positive amyloid PET images, neighboring voxels do not necessarily need to be linearly correlated in either case, especially given that Aβ plaques are present as diffuse deposits [2]. On the contrary, other features like homogeneity that show good performance describe the general similarity of neighboring voxel intensities and show greater differences between Aβ+ and Aβ− cases as demonstrated by ROC analyses.

Comparing the findings of the present study to those by Campbell et al. [22], the authors reported results that state that energy and entropy best discriminate between the studied groups. While these features generally show statistically significant differences in our study, energy in the [^{18}F]FMM group is also one of the three HFs that are not significant when extracted from the global VOI. However, the authors grouped the patients by clinicopathological features and not by Aβ positivity. Moreover, in their study, SUVR showed no statistically significant differences between the groups and HFs performed better, unlike the results presented in this study.

AUC values of ROC curves from features using the global VOI were generally larger than 0.7. Again, correlation is not sufficiently capable of discriminating between Aβ+ and Aβ−. All other features showed overall good performance in ROC analyses of regional VOIs indicating their discriminatory capability and describing correctly the visually identified grey-to-white matter contrast patterns. Overall, an association between the statistically significant group differences in Mann–Whitney U-tests and higher AUC values can be observed. Compared to Campbell et al. [22], the AUC values are generally higher in this study. The authors reported their highest AUC value as 0.695 (energy of the PCC), while in our study it is 0.989 (SUVR of the left temporal VOI). On the other hand, Ben Bouallègue et al. [23] obtained AUC values < 0.75 with HFs in a cross-sectional study group. However, the authors employed a different segmentation method and did not analyze cortical brain regions.

Moreover, ROC analyses show the relationship between the features and Aβ positivity. As mentioned previously, Aβ+ PET images are characterized by a more homogeneous uptake pattern between grey and white matter. Contrast, entropy and dissimilarity result in AUC values <0.3, indicating an inverse relationship to Aβ+. This indicates that features, whose higher values describe heterogeneous spatial intensity distributions, are correlated negatively to Aβ+. On the other hand, energy, homogeneity and correlation show AUC values >0.7. These are features are therefore positively correlated to Aβ+ and their values increase with higher homogeneity of the image intensity values.

Regional group differences have also been detected in statistical testing and ROC analyses. The manuals for visual interpretation of [^{18}F]FBP [9] and [^{18}F]FMM [10] PET images indicate that for a positive diagnosis, at least two or one region needs to present reduced grey-white matter contrast, respectively. Regions of interest defined in those guidelines are the frontal, temporal, and parietal lobes, as well as the posterior cingulate [8–10]. Among all analyses, especially the PCC showed the best results. Good results in the other regions were also obtained in different tests and study groups. For example, the frontal lobe ([^{18}F]FBP) and the temporal lobe ([^{18}F]FMM) can be seen as defining regions between Aβ+ and Aβ− PET images. However, the parietal VOI is the least significant region in our analysis. While it is defined in the guidelines of the visual interpretation, the parietal lobe and higher image slices are more frequently affected by atrophy and therefore might appear to present lower activity in the amyloid PET images. Experienced readers usually focus their analysis on

more caudal slices, which often include the regions with good discriminatory performance in our study. Regarding the quantitative analysis, it has also been shown that the parietal region is particularly prone to artifacts, which could affect the results [36]. Interestingly, the occipital lobe is not included in the regions to review defined by the guidelines for visual interpretation of amyloid PET images but showed good results in our analyses to discriminate between Aβ+ and Aβ− images.

Limitations of this study include the lack of anatomical images for the normalization process and study groups of images with [^{11}C]PiB and [^{18}F]FBB to evaluate HFs in these radiotracers. Additionally, to evaluate the robustness over time of textural features of PET images, longitudinal studies should be performed. In this study, however, only a retrospective cross-sectional study cohort was available. Moreover, a large prospective study cohort would also allow for the calculation of radiotracer-specific cut-off values of the textural parameters for the classification into Aβ+ or Aβ−. Regarding the extracted image features, it should be noted that no standardized protocol for texture analysis in PET images is defined and the intensity quantization method or bin number may vary between studies. Other texture features like those based on image histogram, the grey-level run length matrix or the grey-level size zone matrix or regions like the striatum, which is defined as a region of interest in the visual interpretation of [^{18}F]FMM images [10], could also be evaluated. Lastly, while in this study the individual performance of HFs is analyzed, future studies should include the generation of multivariate classifiers to evaluate the combined performance of image features.

5. Conclusions

PET brain images of amyloid-binding radiotracers are visually interpreted by analyzing grey-to-white-matter contrast. Quantitative image features from PET brain images acquired with [^{18}F]FBP and [^{18}F]FMM are evaluated in this study. SUVRs and HFs from the GLCM are extracted and compared between Aβ+ and Aβ− images. While SUVR still performed better than HFs, these also showed significant differences between the groups. Therefore, it can be concluded that texture features could be an alternative to SUVR that does not need a reference region for its calculation.

Author Contributions: Conceptualization, A.P.S., A.G.-G., E.M., S.L.-V., A.V.-G., E.J.G. and P.S.-G.; methodology, A.P.S., A.G.-G., E.M. and P.S.-G.; software, A.P.S. and E.M.; validation, A.P.S., A.G.-G., E.M., S.L.-V., A.V.-G. and P.S.-G.; formal analysis, A.P.S. and E.M.; investigation, A.P.S., A.G.-G., E.M., S.L.-V., A.V.-G., E.J.G. and P.S.-G.; resources, A.G.-G., S.L.-V., A.V.-G. and E.J.G.; data curation, A.P.S., A.G.-G., E.M., S.L.-V., A.V.-G.; writing—original draft preparation, A.P.S., A.G.-G. and P.S.-G.; writing—review and editing, A.P.S., A.G.-G., E.M., S.L.-V., A.V.-G., E.J.G. and P.S.-G.; visualization, A.P.S. and P.S.-G.; supervision, P.S.-G. All authors have read and agreed to the published version of the manuscript.

Funding: This research received no external funding.

Institutional Review Board Statement: Ethical review and approval were waived for this study, due to involving a retrospective image database.

Informed Consent Statement: Informed consent was obtained from all subjects involved in the study.

Data Availability Statement: The data presented in this study are available on request from the corresponding authors. The data is not publicly available due to clinical patient information.

Acknowledgments: The author A.P.S. received financial support through an FPU Fellowship (Beca de Formación de Profesorado Universitario) from the Spanish Ministry of Science, Innovation and Universities (FPU16/06487). The author A.G.-G. is a researcher-PhD student at the Department of Radiology of the Facultad de Medicina (Medical School) of the Universidad Complutense de Madrid, Madrid, Spain. The author S.L.-V. is supported by the Instituto de Salud Carlos III (ISCIII; Spanish Biomedical Research Institute) through a "Juan Rodés" contract (JR 18/00046).

Conflicts of Interest: The authors declare no conflict of interest.

References

1. Jack, C.R.; Bennett, D.A.; Blennow, K.; Carrillo, M.C.; Dunn, B.; Haeberlein, S.B.; Holtzman, D.M.; Jagust, W.; Jessen, F.; Karlawish, J.; et al. NIA-AA Research Framework: Toward a biological definition of Alzheimer's disease. *Alzheimer's Dement.* **2018**, *14*, 535–562. [CrossRef] [PubMed]
2. Chen, G.F.; Xu, T.H.; Yan, Y.; Zhou, Y.R.; Jiang, Y.; Melcher, K.; Xu, H.E. Amyloid beta: Structure, biology and structure-based therapeutic development. *Acta Pharmacol. Sin.* **2017**, *38*, 1205–1235. [CrossRef] [PubMed]
3. Ikonomovic, M.D.; Klunk, W.E.; Abrahamson, E.E.; Mathis, C.A.; Price, J.C.; Tsopelas, N.D.; Lopresti, B.J.; Ziolko, S.; Bi, W.; Paljug, W.R.; et al. Post-mortem correlates of in vivo PiB-PET amyloid imaging in a typical case of Alzheimer's disease. *Brain* **2008**, *131*, 1630–1645. [CrossRef]
4. Clark, C.M.; Pontecorvo, M.J.; Beach, T.G.; Bedell, B.J.; Coleman, R.E.; Doraiswamy, P.M.; Fleisher, A.S.; Reiman, E.M.; Sabbagh, M.N.; Sadowsky, C.H.; et al. Cerebral PET with florbetapir compared with neuropathology at autopsy for detection of neuritic amyloid-β plaques: A prospective cohort study. *Lancet Neurol.* **2012**, *11*, 669–678. [CrossRef]
5. Sabri, O.; Sabbagh, M.N.; Seibyl, J.; Barthel, H.; Akatsu, H.; Ouchi, Y.; Senda, K.; Murayama, S.; Ishii, K.; Takao, M.; et al. Florbetaben PET imaging to detect amyloid beta plaques in Alzheimer's disease: Phase 3 study. *Alzheimer's Dement.* **2015**, *11*, 964–974. [CrossRef]
6. Curtis, C.; Gamez, J.E.; Singh, U.; Sadowsky, C.H.; Villena, T.; Sabbagh, M.N.; Beach, T.G.; Duara, R.; Fleisher, A.S.; Frey, K.A.; et al. Phase 3 trial of flutemetamol labeled with radioactive fluorine 18 imaging and neuritic plaque density. *JAMA Neurol.* **2015**, *72*, 287–294. [CrossRef]
7. Tiepolt, S.; Patt, M.; Aghakhanyan, G.; Meyer, P.M.; Hesse, S.; Barthel, H.; Sabri, O. Current radiotracers to image neurodegenerative diseases. *EJNMMI Radiopharm. Chem.* **2019**, *4*, 17. [CrossRef] [PubMed]
8. Minoshima, S.; Drzezga, A.E.; Barthel, H.; Bohnen, N.; Djekidel, M.; Lewis, D.H.; Mathis, C.A.; McConathy, J.; Nordberg, A.; Sabri, O.; et al. SNMMI procedure standard/EANM practice guideline for amyloid PET imaging of the brain 1.0. *J. Nucl. Med.* **2016**, *57*, 1316–1322. [CrossRef]
9. Trembath, L.A.; Newell, M.; Devous, M.D. Technical considerations in brain amyloid PET imaging with 18F-Florbetapir. *J. Nucl. Med. Technol.* **2015**, *43*, 175–184. [CrossRef] [PubMed]
10. GE Healthcare VizamylTM, Flutemetamol F 18 Injection. Available online: http://www3.gehealthcare.com/~/media/documents/us-global/products/nuclear-imaging-agents_non-gatekeeper/clinicalproductinfo/vizamyl/gehealthcare-vizamyl-prescribing-information.pdf (accessed on 13 February 2021).
11. Morris, E.; Chalkidou, A.; Hammers, A.; Peacock, J.; Summers, J.; Keevil, S. Diagnostic accuracy of 18F amyloid PET tracers for the diagnosis of Alzheimer's disease: A systematic review and meta-analysis. *Eur. J. Nucl. Med. Mol. Imaging* **2016**, *43*, 374–385. [CrossRef]
12. Villeneuve, S.; Rabinovici, G.D.; Cohn-Sheehy, B.I.; Madison, C.; Ayakta, N.; Ghosh, P.M.; La Joie, R.; Arthur-Bentil, S.K.; Vogel, J.W.; Marks, S.M.; et al. Existing Pittsburgh Compound-B positron emission tomography thresholds are too high: Statistical and pathological evaluation. *Brain* **2015**, *138*, 2020–2033. [CrossRef]
13. Joshi, A.D.; Pontecorvo, M.J.; Clark, C.M.; Carpenter, A.P.; Jennings, D.L.; Sadowsky, C.H.; Adler, L.P.; Kovnat, K.D.; Seibyl, J.P.; Arora, A.; et al. Performance characteristics of amyloid PET with florbetapir F 18 in patients with Alzheimer's disease and cognitively normal subjects. *J. Nucl. Med.* **2012**, *53*, 378–384. [CrossRef]
14. Thurfjell, L.; Lilja, J.; Lundqvist, R.; Buckley, C.; Smith, A.; Vandenberghe, R.; Sherwin, P. Automated quantification of 18F-flutemetamol PET activity for categorizing scans as negative or positive for brain amyloid: Concordance with visual image reads. *J. Nucl. Med.* **2014**, *55*, 1623–1628. [CrossRef]
15. Lin, K.J.; Hsiao, I.T.; Hsu, J.L.; Huang, C.C.; Huang, K.L.; Hsieh, C.J.; Wey, S.P.; Yen, T.C. Imaging characteristic of dual-phase 18F-florbetapir (AV-45/Amyvid) PET for the concomitant detection of perfusion deficits and beta-amyloid deposition in Alzheimer's disease and mild cognitive impairment. *Eur. J. Nucl. Med. Mol. Imaging* **2016**, *43*, 1304–1314. [CrossRef] [PubMed]
16. Landau, S.M.; Fero, A.; Baker, S.L.; Koeppe, R.; Mintun, M.; Chen, K.; Reiman, E.M.; Jagust, W.J. Measurement of longitudinal β-amyloid change with 18F-florbetapir PET and standardized uptake value ratios. *J. Nucl. Med.* **2015**, *56*, 567–574. [CrossRef]
17. Blautzik, J.; Brendel, M.; Sauerbeck, J.; Kotz, S.; Scheiwein, F.; Bartenstein, P.; Seibyl, J.; Rominger, A. Reference region selection and the association between the rate of amyloid accumulation over time and the baseline amyloid burden. *Eur. J. Nucl. Med. Mol. Imaging* **2017**, *44*, 1364–1374. [CrossRef]
18. Bullich, S.; Villemagne, V.L.; Catafau, A.M.; Jovalekic, A.; Koglin, N.; Rowe, C.C.; De Santi, S. Optimal reference region to measure longitudinal amyloid-b change with 18F-Florbetaben PET. *J. Nucl. Med.* **2017**, *58*, 1300–1306. [CrossRef]
19. Lowe, V.J.; Lundt, E.S.; Senjem, M.L.; Schwarz, C.G.; Min, H.K.; Przybelski, S.A.; Kantarci, K.; Knopman, D.; Petersen, R.C.; Jack, C.R. White matter reference region in PET studies of 11C-Pittsburgh compound B uptake: Effects of age and amyloid-β deposition. *J. Nucl. Med.* **2018**, *59*, 1583–1589. [CrossRef] [PubMed]
20. Cho, S.H.; Choe, Y.S.; Park, S.; Kim, Y.J.; Kim, H.J.; Jang, H.; Kim, S.J.; Kim, J.P.; Jung, Y.H.; Kim, B.C.; et al. Appropriate reference region selection of 18F-florbetaben and 18F-flutemetamol beta-amyloid PET expressed in Centiloid. *Sci. Rep.* **2020**, *10*, 14950. [CrossRef]
21. Whittington, A.; Gunn, R.N. Amyloid load: A more sensitive biomarker for amyloid imaging. *J. Nucl. Med.* **2019**, *60*, 536–540. [CrossRef]

22. Campbell, D.L.; Kang, H.; Shokouhi, S. Application of Haralick texture features in brain [18F]-florbetapir positron emission tomography without reference region normalization. *Clin. Interv. Aging* **2017**, *12*, 2077–2086. [CrossRef]
23. Ben Bouallègue, F.; Vauchot, F.; Mariano-Goulart, D.; Payoux, P. Diagnostic and prognostic value of amyloid PET textural and shape features: Comparison with classical semi-quantitative rating in 760 patients from the ADNI-2 database. *Brain Imaging Behav.* **2019**, *13*, 111–125. [CrossRef]
24. Haralick, R.M.; Dinstein, I.; Shanmugam, K. Textural Features for Image Classification. *IEEE Trans. Syst. Man Cybern.* **1973**, *3*, 610–621. [CrossRef]
25. Friston, K.J.; Ashburner, J.; Kiebel, S.; Nichols, T.; Penny, W.D. *Statistical Parametric Mapping: The Analysis of Funtional Brain Images*, 1st ed.; Elsevier: Amsterdam, The Netherlands; Academic Press: London, UK, 2006; ISBN 9780080466507.
26. Presotto, L.; Iaccarino, L.; Sala, A.; Vanoli, E.G.; Muscio, C.; Nigri, A.; Bruzzone, M.G.; Tagliavini, F.; Gianolli, L.; Perani, D.; et al. Low-dose CT for the spatial normalization of PET images: A validation procedure for amyloid-PET semi-quantification. *NeuroImage Clin.* **2018**, *20*, 153–160. [CrossRef]
27. Tzourio-Mazoyer, N.; Landeau, B.; Papathanassiou, D.; Crivello, F.; Etard, O.; Delcroix, N.; Mazoyer, B.; Joliot, M. Automated anatomical labeling of activations in SPM using a macroscopic anatomical parcellation of the MNI MRI single-subject brain. *Neuroimage* **2002**, *15*, 273–289. [CrossRef] [PubMed]
28. Rolls, E.T.; Joliot, M.; Tzourio-Mazoyer, N. Implementation of a new parcellation of the orbitofrontal cortex in the automated anatomical labeling atlas. *Neuroimage* **2015**, *122*, 1–5. [CrossRef]
29. Frings, L.; Hellwig, S.; Spehl, T.S.; Bormann, T.; Buchert, R.; Vach, W.; Minkova, L.; Heimbach, B.; Klöppel, S.; Meyer, P.T. Asymmetries of amyloid-β burden and neuronal dysfunction are positively correlated in Alzheimer's disease. *Brain* **2015**, *138*, 3089–3099. [CrossRef]
30. Sacher, C.; Blume, T.; Beyer, L.; Biechele, G.; Sauerbeck, J.; Eckenweber, F.; Deussing, M.; Focke, C.; Parhizkar, S.; Lindner, S.; et al. Asymmetry of Fibrillar Plaque Burden in Amyloid Mouse Models. *J. Nucl. Med.* **2020**, *61*, 1825–1831. [CrossRef] [PubMed]
31. Vallières, M.; Freeman, C.R.; Skamene, S.R.; El Naqa, I. A radiomics model from joint FDG-PET and MRI texture features for the prediction of lung metastases in soft-tissue sarcomas of the extremities. *Phys. Med. Biol.* **2015**, *60*, 5471–5496. [CrossRef] [PubMed]
32. Zhou, H.; Vallières, M.; Bai, H.X.; Su, C.; Tang, H.; Oldridge, D.; Zhang, Z.; Xiao, B.; Liao, W.; Tao, Y.; et al. MRI features predict survival and molecular markers in diffuse lower-grade gliomas. *Neuro. Oncol.* **2017**, *19*, 862–870. [CrossRef]
33. Vallières, M.; Kay-Rivest, E.; Perrin, L.J.; Liem, X.; Furstoss, C.; Aerts, H.J.W.L.; Khaouam, N.; Nguyen-Tan, P.F.; Wang, C.S.; Sultanem, K.; et al. Radiomics strategies for risk assessment of tumour failure in head-and-neck cancer. *Sci. Rep.* **2017**, *7*, 10117. [CrossRef] [PubMed]
34. Johnson, K.A.; Sperling, R.A.; Gidicsin, C.M.; Carmasin, J.S.; Maye, J.E.; Coleman, R.E.; Reiman, E.M.; Sabbagh, M.N.; Sadowsky, C.H.; Fleisher, A.S.; et al. Florbetapir (F18-AV-45) PET to assess amyloid burden in Alzheimer's disease dementia, mild cognitive impairment, and normal aging. *Alzheimer's Dement.* **2013**, *9*, S72–S83. [CrossRef] [PubMed]
35. Hosmer, D.W.; Lemeshow, S.; Sturdivant, R.X. Assessing the Fit of the Model. In *Applied Logistic Regression*; John Wiley & Sons: Hoboken, NJ, USA, 2013; pp. 153–225.
36. Högenauer, M.; Brendel, M.; Delker, A.; Därr, S.; Weiss, M.; Bartenstein, P.; Rominger, A. Impact of MRI-based Segmentation Artifacts on Amyloid- and FDG-PET Quantitation. *Curr. Alzheimer Res.* **2016**, *13*, 597–607. [CrossRef] [PubMed]